A new ignition scheme using hybrid indirect-direct drive for inertial confinement fusion

Zhengfeng Fan (范征锋),[1,*] Mo Chen (陈默),[1] Zhensheng Dai (戴振生),[1] Hong-bo Cai (蔡洪波),[1] Shao-ping Zhu (朱少平),[1] W. Y. Zhang (张维岩),[1] and X. T. He (贺贤土)[1,2,†]

[1] *Institute of Applied Physics and Computational Mathematics, Beijing 100088, China*
[2] *Center for Applied Physics and Technology, Peking University, Beijing 100871, China*

A new hybrid indirect-direct-drive ignition scheme is proposed for inertial confinement fusion: a cryogenic capsule encased in a hohlraum is first compressed symmetrically by indirect-drive x-rays, and then accelerated and ignited by both direct-drive lasers and x-rays. A steady high density plateau newly formed between the radiation and electron ablation fronts suppresses the rarefaction at the radiation ablation front and greatly enhances the drive pressure. Meanwhile, multiple shock reflections at the fuel/hot-spot interface are prevented during capsule deceleration. Thus rapid ignition and burn are realized. In comparison with the conventional indirect drive, the hybrid drive implodes the capsule with a higher velocity ($\sim 4.3 \times 10^7$ cm/s) and a much lower convergence ratio ($\sim$25), and the growth of hydrodynamic instabilities is significantly reduced, especially at the fuel/hot-spot interface.

PACS numbers: 52.57.-z, 28.52.Cx

In central hot spot ignition scheme of inertial confinement fusion (ICF) [1–3], a spherical capsule which is composed of deuterium-tritium (DT) gas, DT fuel and an ablator, is cryogenically imploded to a high velocity, then the DT fuel is highly compressed and a hot spot is formed at the capsule center due to spherical convergent compression effect. When the alpha-particle heating of the hot spot exceeds the total energy losses, central ignition occurs and a burn wave propagates into the surrounding cold fuel. Two main implosion schemes, direct drive [4] and indirect drive [5], have been proposed for realizing central hot spot ignition. The National Ignition Campaign (NIC) [6] experiments have made great progresses towards ignition using indirect-drive targets. For example, the National Ignition Facility is now capable of delivering 1.9 MJ of 0.35-μm laser light at 500 TW, and the assembled fuel areal density has reached about 1.3 g/cm^2 which is 80 percent of the ignition goal [7, 8]. However, the NIC experiments are facing challenges, and the experimental ignition threshold factor which is a metric of the progress towards ignition needs to be increased by an order of magnitude to meet the ignition requirement. Besides laser plasma instabilities (LPI), two major issues in implosion dynamics are: (1) a strong rarefaction wave generated from the expansion of the radiation ablated plasmas seriously decreases the ablation pressure and limits the possibility of increasing implosion velocity; (2) hydrodynamic instabilities are more severe than predicted causing hot spot asymmetry and material mixing, and one of the important reasons for this is multiple shock reflections at the fuel/hot-spot interface during the deceleration phase.

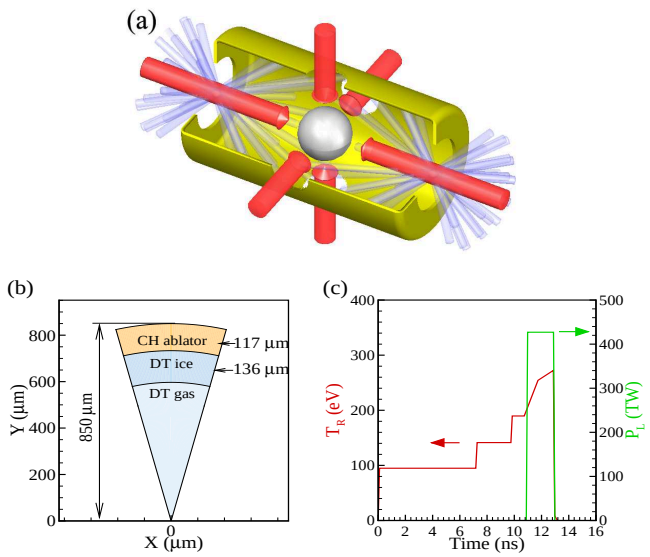

FIG. 1: (Color online). (a) Schematic of the hybrid-drive ignition target configuration; (b) capsule cross-section; and (c) indirect-drive radiation temperature (red) and direct-drive laser power (green) vs time.

In this Letter, to overcome the above issues, we propose a new hybrid indirect-direct-drive ignition scheme, whose configuration is shown in Fig. 1(a). A cryogenic ignition capsule encased at the center of a normal cylindrical high-Z hohlraum is first compressed symmetrically on a low adiabat by x-rays converted from indirect-drive laser beams through two laser-entrance holes (LEHs) at opposite ends. Then six clusters of direct laser beams are incident straightly on the capsule through the two LEHs at the ends and four additional symmetrical cylinder-like laser channels at the waist. The hybrid indirect-direct drive accelerates and finally ignites the capsule. This scheme is different from the previous hybrid-drive concept [9] in which an initial x-ray pulse is used for suppressing initial laser imprints by preheating, but not during the implosion and ignition. As compared with the recently proposed shock ignition scheme in which the compression and ignition steps are separated and both adopt direct-drive lasers [10–14], our hybrid-drive scheme launches direct laser beams simultaneously with the main pulse of the indirect drive, which creates a double-ablation-front (DAF) structure consisting of a radiation ablation front (RAF) and an electron ablation front (EAF). Between the two fronts, a nearly steady high density plateau is formed, which suppresses the rarefaction at the RAF and greatly enhances the drive pressure. The enhanced drive pressure pushes the capsule to a higher implosion velocity and quickens the hot spot formation via inward shock/compression waves. Meanwhile, the convergence ratio is kept at a lower level. The hybrid-drive scheme can smooth the imprints and drive asymmetries of direct lasers by keeping the critical surface in the corona at a proper distance away from the capsule, and more beneficially, hydrodynamic instabilities are greatly stabilized even by comparison with the conventional indirect drive

as in the point design target (PT) [15] in the NIC mission.

To illustrate our new scheme, we investigate implosion dynamics of a typical ignition capsule with an outer radius of 850 μm, about 4/5 of the PT [15] in the NIC mission. This capsule requires a total drive laser energy of ∼1.35 MJ, which is also a representative value for the PT. Figure 1(b) shows the cross-section of the typical capsule. The CH ablator of the capsule has a 117 μm thickness with a density of 1.0 g/cm^3 and a mass of 0.92 mg, while the solid DT fuel layer has a 136 μm thickness with a density of 0.25 g/cm^3 and a mass of 0.19 mg. The density of the DT filling gas is 0.3 mg/cm^3. The total mass of this capsule is about 1.11 mg. Figure 1(c) plots the given radiation drive temperature and direct-drive laser power. The peak radiation temperature is 270 eV, and the estimated indirect laser energy is about 500 kJ by assuming a coupling efficiency of 10% from laser to capsule absorption. The drive pulse of the radiation temperature has four steps at 0.0, 7.2, 9.8 and 10.7 ns. These steps create four successive shocks whose timing follows the Munro criteria [16]. During the rise time of the fourth step (the main pulse), direct-drive laser beams are launched. The direct laser pulse at λ =0.35 μm and 425 TW has only one single step with a duration of 2 ns and total energy of 850 kJ. The absorbed laser intensity near the critical surface (its radius is ∼1000 μm) is about 3.4 × 10^{15} W/cm^2.

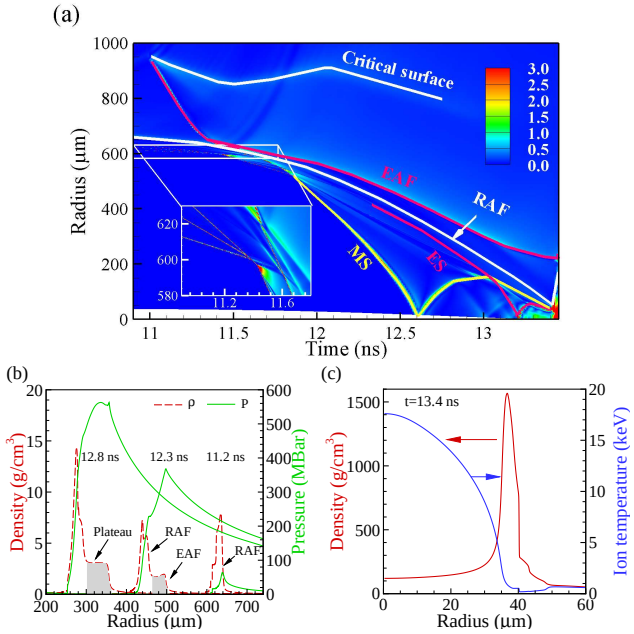

FIG. 2: (Color online). (a) Contours of the fluid velocity gradient ($|\nabla u|$) in the space-time plane, the subpanel magnifies the four shocks of the indirect drive; (b) the density and pressure profiles at t = 11.2 ns (with the RAF only), 12.3 ns and 12.8 ns (with both the RAF and EAF); and (c) the density and ion temperature profiles at stagnation t = 13.4 ns. The EAF, RAF, MS and ES are the abbreviations of electron ablation front, radiation ablation front, merged shock and enhancement shock, respectively.

Capsule implosion dynamics simulations are performed using the radiation-hydrodynamics code LARED-S [17], which is multi-dimensional, massively parallel and Eulerian mesh based. Multiphysics in the current simulations include laser ray tracing, multi-group radiation diffusion (20 groups), plasma hydrodynamics, electron and ion thermal conductions, nuclear reaction, alpha particle transport, and the quotidian equations of state [18]. In this Letter, our discussions only focus on the implosion dynamics, while LPI involving stimulated Brillouin scattering, stimulated Raman scattering, two-plasmon decay, etc., which would reduce the absorption rate of the direct-drive laser energy and generate superthermal electrons preheating the DT fuel, have been discussed elsewhere [19–21].

Figure 2(a) shows the implosion and ignition processes calculated by one-dimensional (1D) simulations, using 2000 meshes with a minimum grid size of 0.05 μm. The first three shocks of indirect drive merge at the inner surface of the DT fuel layer at time t = 11.4 ns, and the fourth shock chases them, as shown in the subpanel of Fig. 2(a). Direct lasers launched at t = 10.9 ns deposit energy in the vicinity of the critical surface which is kept about 300 μm away from the capsule. The electron temperature in this region rapidly rises to a maximum of about 7 keV, and an EAF generated by electron thermal conduction propagates towards the RAF with a supersonic speed of ∼8.4 × 10^7 cm/s. When approaching the RAF at about t = 11.5 ns, the EAF slows down to a subsonic speed and drives an

electron thermal shock which travels into the capsule and forms a merged shock (MS) with the previous four shocks. After $t = 11.5$ ns, the EAF and RAF separate from each other due to their different mass ablation rates, and hence a DAF structure is formed. The EAF compresses the ablated rarefaction plasmas behind the RAF like a piston, so that the rarefaction effect from the conventional indirect drive is controlled and a nearly steady density plateau with tens of microns width is created, see gray regions in Fig. 2(b). The density is enhanced from $\sim$0.2 g/cm^3 at t = 11.2 ns to 1.5$\sim$2.0 g/cm^3 at $t = 12.3$ ns, and correspondingly the pressure at the RAF is significantly increased from $\sim$60 MBar to $\sim$230 MBar, as shown in Fig. 2(b). During the implosion process, the drive pressure is further increased as the capsule converges, with an average value of 450 MBar from $t = 11.5$ to 13.2 ns, leading to a maximum implosion velocity of 4.25×10^7 cm/s. Comparing with the PT [15] in the NIC mission, at equivalent total drive energy of $\sim$1.35 MJ, the (maximum) implosion velocity of our hybrid-drive capsule is about 15% higher. Meanwhile, the increasing drive pressure produces a series of compression waves forming an enhancement shock (ES) at about t = 12.3 ns. The ES collides with the rebounded MS near the fuel/hot-spot interface generating an inward shock and an outward one. At about $t = 13.2$ ns, the inward shock arrives at the capsule center, quickly raises the hot spot temperature and pressure, and leads to a lower convergence ratio of 25. The hot spot rapidly achieves the ignition condition soon after the first shock reflection ($\sim$13.3 ns) at the fuel/hot-spot interface. If the ES does not exist as in the conventional indirect drive, there would have multiple shock reflections at the fuel/hot-spot interface followed by severe Rayleigh-Taylor instability (RTI) growth. Figure 2(c) shows the stagnation density and temperature profiles at about $t = 13.4$ ns. The corresponding peak fuel density, the hot spot areal density and hot spot average ion temperature are 1560 g/cm^3, 0.59 g/cm^2 and 8.8 keV, respectively. Finally, the DT fuel burns, achieving an energy yield of 17.4 MJ and an energy gain of 13.

The drive asymmetry of the hybrid-drive ignition scheme originates from both the x-ray drive and direct laser drive. An additional x-ray drive asymmetry caused by four cylinder-like direct laser channels may is same as the conventional indirect drive. Notice that the velocity of the critical surface on the 0.35-μm laser spots irradiated at the inner wall of the hohlraum is 10 μm/ns at most, which can be seen in Fig. 2(a) as well, where the critical surface moves from the initial position of 850 μm at the outer surface of the capsule to the place of $\sim$950 μm within about 13 ns. Thus, it can avert the influence of overdense plasma to impact four cylinder-like structures if we insert the cylinder bottoms (each one packed a thin ablative layer) into the hohlraum as long as in a little depth of $\sim$150-200 μm which is only $\sim$4% for the hohlraum radius of $\sim$4500-5000 μm. On the other hand, because of the little depth it may be easy to tune the indirect-drive laser beam uniformity to be close to the conventional indirect drive. In the real target design, of course we must do it with the help of both 3D simulations and experiments. In this Letter, we focus on the intrinsic low-mode asymmetries of direct drive caused by the six limited incident directions. The high-mode asymmetries can be smoothed during inward propagation of electron thermal conduction because the critical surface is kept hundreds of microns away from the capsule. A 3D ray-tracing package is used to calculate the energy deposition and evaluate the asymmetries, supposing that the laser intensity ($\sim 3.4 \times 10^{15}$ W/cm^2) of each cluster is uniform. Figure 3(a) shows the distribution of absorbed laser intensities along the polar angle θ and the azimuthal angle ϕ obtained at a typical time $t = 12.0$ ns using about one million laser rays, and the peak-to-valley ratio is 1.27. Spherical harmonics expansion indicates that the main modes are $Y_{4,\pm4}$ and $Y_{4,0}$ with amplitudes of $Y_{4,\pm4}/Y_{0,0}$ = -2.6% and $Y_{4,0}/Y_{0,0}$ = -4.2%, respectively. Strictly speaking, accurate evaluation of the intrinsic low-mode drive asymmetries needs 3D simulations which are computationally expensive. Instead, we perform two-dimensional (2D) implosion dynamics simulations with the $Y_{6,0}$ mode to approximate the 3D behavior, and the equivalent amplitude matching the peak-to-valley ratio of 1.27 is $Y_{6,0}/Y_{0,0} \approx$ -4.5%. Figure 3(b) plots the corresponding 2D density contour at stagnation. The capsule seems spherical, and the peak-to-valley amplitude at the fuel/hot-spot interface is 0.9 μm, about 2.6% of the hot spot radius. The average hot spot areal density and ion temperature are close to the 1D results, and the yield over clean (the ratio of the 2D neutron yield to the 1D yield) is almost 1.0. This means that the deformation of the hot spot has limited effects on the ignition. Therefore, the primary investigation indicates that the asymmetry of the direct drive in the hybrid-drive scheme is tolerable.

The hybrid-drive ignition features lower growth of hydrodynamic instabilities. To demonstrate this, we compare the hybrid-drive ignition target with an indirect-drive PT similar to that presented in Ref. [5]. The PT target has an outer radius of 1110 μm with a 160 μm CH ablator and 80 μm solid DT fuel. The profile of radiation temperature for the PT is similar to that of the hybrid-drive ignition target, with the levels of the first three steps equal to those of the hybrid-drive target and the peak temperature of 300 eV. The laser energy requirement is about 1.35 MJ, equivalent to that of our hybrid-drive target. 1D simulations indicate that the implosion velocity of the PT is about 3.8×10^7 cm/s, and the thermonuclear energy yield is 16 MJ. Then we perform a series of 2D single-mode simulations with the mode number L ranging from 4 to 40. The perturbations are initially seeded on the ablator outer surface. In order to save computation time, the simulations are done on wedges with angles $\theta \in [\pi/2 - \pi/L, \pi/2 + \pi/L]$, and 50 meshes are used in the angular direction.

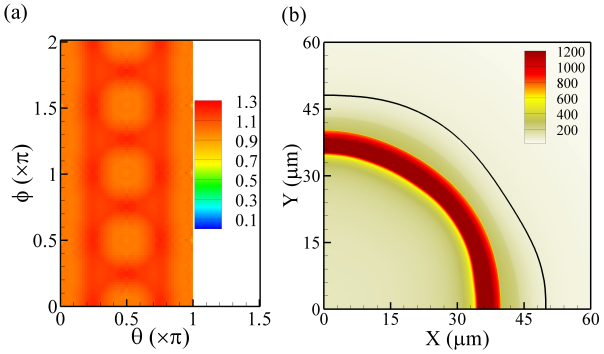

FIG. 3: (Color online) 2D drive asymmetry of direct drive in the hybrid-drive target. (a) Distribution of the absorbed laser intensity normalized to the intensity of direct-drive laser, where θ is the polar angle and ϕ is the azimuthal angle; (b) density contour at stagnation time for direct-drive asymmetry with $Y_{6,0}/Y_{0,0}$ = -4.5%, where the black curve is the ablator/fuel interface.

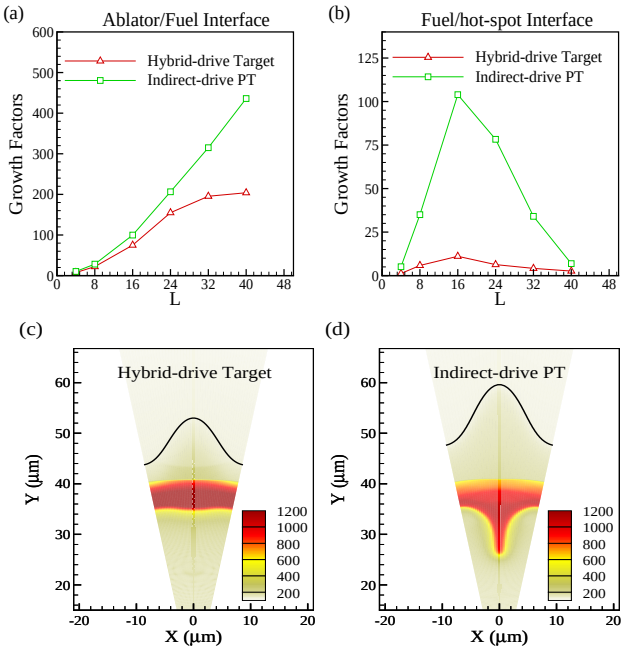

FIG. 4: (Color online) Comparisons of the growth of hydrodynamic instabilities between the hybrid-drive target and the indirect-drive PT for perturbations initially seeded at the ablator outer surface. Growth factors (a) to the ablator/fuel interface and (b) to the fuel/hot-spot interface, at stagnation times. Density contours for a perturbation with a mode $L = 16$ and an initial roughness of 350 Å (c) for the hybrid-drive target, and (d) for the PT, at stagnation times. In (c) and (d), the black curves are the ablator/fuel interfaces.

First, perturbation growth to the ablator/fuel interface is reduced in the hybrid-drive target as compared with that in the PT, as shown in Fig. 4(a). During the acceleration stage of the capsule implosion, i.e. $t \in [11.5, 13.2]$ ns, the DAF structure reduces the Atwood number at the RAF to an average of 0.63. The reduced Atwood number decreases the perturbation growth, since the RTI growth is approximated by the modified Lindl formula $\gamma = \sqrt{A_t kg/(1 + A_t kL)} - \beta k V_a$ [22], where A_t, k, g, L, V_a and β are the Atwood number, wave number, acceleration, minimum density gradient scale length, ablation velocity and a constant, respectively.

Second, perturbation growth to the fuel/hot-spot interface is significantly reduced in the hybrid-drive target as compared with that in the PT, as shown in Fig. 4(b). During the deceleration stage of the PT, a merged shock reflects twice (or even more) off the fuel/hot-spot interface in the PT leading to an early reverse of the pressure gradient (i.e. $\nabla p \cdot \nabla \rho < 0$) and causing severe growth of RTI. However, in the hybrid-drive target, the collision of

the ES with the rebounded MS delays the reverse of the pressure gradient, and a higher hot spot temperature also enhances the stabilization of deceleration phase RTI. For the mode $L = 16$, which has the maximum growth of all the modes, the growth is reduced by an order of magnitude in the hybrid-drive target, as compared with that in the PT. Figures 4(c) and 4(d) compare the density contours at stagnation times between the hybrid-drive target and the PT, for the $L = 16$ mode with an initial roughness of 350 $\mathring{A}$. The bubble and spike structures at the fuel/hot-spot interface are much smaller in the hybrid-drive target than those in the PT. The lower level growth of hydrodynamic instabilities means that the hybrid-drive target is more robust than the indirect-drive PT, and this is essential for realizing ignition in ICF.

In summary, we have proposed a new hybrid-drive ignition scheme coupling both indirect drive and direct drive. Higher drive pressure ($\sim$450 Mbar) and implosion velocity ($\sim 4.3 \times 10^7$ cm/s) are obtained due to a high density plateau between the RAF and EAF. The ignition process is quickened and the convergence ratio is much lower ($\sim$25). It is found that 2D simulation results with intrinsic low-mode asymmetry of direct drive are close to the 1D results. More importantly, the hybrid drive scheme features lower growth of hydrodynamic instability, especially at the fuel/hot-spot interface where the perturbation is reduced almost by an order of magnitude. Because of high laser intensities ($\sim 3.4 \times 10^{15}$ W/cm^2) in the direct drive, the LPI need to be concerned in the future.

The authors are grateful to L. J. Perkins and Dongguo Kang for beneficial discussions. This work has been supported by the National ICF program of China, the National Basic Research Program of China (No. 2013CB34100), the National High Technology Research and Development Program of China (No. 2012AA01A303) and the National Natural Science Foundation of China (Grant Nos. 10905006, 10935003, 11075024, 91130002, 11105016 and 11205017).

* Electronic address: zffan@yahoo.com.cn
† xthe@iapcm.ac.cn

[1] J. Nuckolls *et al.*, Nature (London) **239**, 139 (1972).
[2] J. D. Lindl, *Inertial Confinement Fusion* (Springer, New York, 1998).
[3] S. Atzeni and J. Meyer-ter-Vehn, *The Physics of Inertial Fusion* (Clarendon Press, Oxford, 2004).
[4] S. E. Bodner *et al.*, Phys. Plasmas **5**, 1901 (1998).
[5] J. D. Lindl *et al.*, Phys. Plasmas **11**, 339 (2004).
[6] E. Moses and C. R. Wuest, Fusion Sci. Technol. **47**, 314 (2005).
[7] A. J. Mackinnon *et al.*, Phys. Rev. Lett. **108**, 215005 (2012).
[8] O. L. Landen *et al.*, Plasma Phys. Control. Fusion **54**, 124026 (2012).
[9] H. Nishimura *et al.*, Nucl. Fusion **40**, 547 (2000).
[10] R. Betti *et al.*, Phys. Rev. Lett. **98**, 155001 (2007).
[11] L. J. Perkins *et al.*, Phys. Rev. Lett. **103**, 045004 (2009).
[12] X. Ribeyre *et al.*, Plasma Phys. Control. Fusion **51**, 015013 (2009).
[13] A. J. Schmitt *et al.*, Phys. Plasmas **17**, 042701 (2010).
[14] S. Atzeni *et al.*, Phys. Plasmas **19**, 090702 (2012).
[15] S. W. Haan *et al.*, Phys. Plasmas **18**, 051001 (2011).
[16] D. H. Munro *et al.*, Phys. Plasmas **8**, 2245 (2001).
[17] W. B. Pei *et al.*, Commun. Comput. Phys. **2**, 255 (2007).
[18] R. M. More *et al.*, Phys. Fluids **31**, 3059 (1988).
[19] S. Depierreux *et al.*, Plasma Phys. Control. Fusion **53**, 124034 (2011).
[20] D. H. Froula *et al.*, Plasma Phys. Control. Fusion **54**, 124016 (2012).
[21] M. R. Terry, L. J. Perkins, and S. M. Sepke, Phys. Plasmas **19**, 112705 (2012).
[22] W. H. Ye, W. Y. Zhang, and X. T. He, Phys. Rev. E **65**, 057401 (2002).